Journal of Sound and Vibration (2001) **243**(2), 215–240
doi:10.1006/jsvi.2000.3408, available online at http://www.idealibrary.com on IDEAL®

NUMERICAL INVESTIGATION OF A ROTOR SYSTEM WITH DISC-HOUSING IMPACT

J. ZAPOMĚL

Department of Mechanics, VŠB-Technical University of Ostrava, 17 *Listopadu* 15, 708 33 *Ostrava - Poruba, Czech Republic*

C. H. J. FOX

School of Mechanical Engineering, University of Nottingham, England

AND

E. MALENOVSKÝ

Institute of Mechanics of Solids, Technical University of Brno, Technická 2, *Brno, Czech Republic*

(*Received* 17 *January* 2000, *and in final form* 27 *June* 2000)

This paper presents a computer modelling investigation of the dynamic behaviour of rotors supported by hydrodynamic bearings. The rotor is discretized into finite elements. The fluid-film bearings are represented by non-linear forces that are linearized in the neighbourhood of the static equilibrium position. Particular emphasis is given to the modelling of impacts between rotor discs and their casings, for which two approaches are used, namely (i) Newton's impact theory and (ii) direct determination of contact forces using a contact stiffness. In the first approach, the discs are assumed to be connected to the shaft by spring elements. The discs and the stationary part are considered to be absolutely rigid. Velocity components of the discs after the impact are calculated using the law of conservation of the momentum and moment of momentum. Dissipation of mechanical energy during impact is taken into account through the coefficient of restitution. In the second approach local flexibility and damping in the contact area are assumed. Local deformation produces impact forces and moments acting on the shaft at the disc location. In both cases, Coulomb friction is assumed to act in the contact area. A modified form of the Newmark method was applied to solve the resulting non-linear equations of motion. Both approaches make it possible to characterize the steady state forced vibration behaviour (periodic, quasi-periodic, chaotic). In addition, the second approach provides further information on the likely magnitude and time history of the impact forces, duration of impacts, etc. The two approaches are illustrated by examples involving imbalance excitation and kinematic excitation of the baseplate.

1. INTRODUCTION

To ensure efficient performance, the radial clearance between the rotating and the stationary parts in rotating machinery is usually small. Consequently, lateral vibration of the shaft can result in contact between the rotor discs and the stator. Friction forces acting in the contact area produce local heating and considerable wear, and such working conditions can lead to serious failure of the machinery.

For investigation of this phenomenon, computer-modelling methods can be applied, and researchers have analyzed flexible rotor-systems using many different approaches. Some have utilized continuous models, but these are rather often complicated, even if the model is

linear. Others have represented the shaft as a beam-like body, discretized into finite elements for which appropriate stiffness, inertia, gyroscopic and damping matrices are derived in references [1, 2], taking into account the rotation of the rotor.

Computational models for hydordynamic bearings have been presented in a large number of publications. The commonly accepted assumptions on which the theory of fluid-film bearings is based are summarized in references [3, 4]. The bearings are usually represented as non-linear force couplings between rotor and stator. In cases where the displacements and velocities of the journal centre from the state of equilibrium are not large, the bearing forces are often linearized in the neighbourhood of the equilibrium position to simplify the solution of the equation of motion. Linearization of bearing forces is described in references [3, 4].

Impact of the rotor on the stationary part causes non-linear behaviour of the system. It has been observed both numerically and experimentally [5] that, even if the excitation is a periodic function of time, the induced vibration can be not only periodic, but also quasi-periodic or chaotic in character. The resulting rotor motion can be viewed in various ways, including orbit plots, Fourier transforms of time series of the response, and Poincaré maps [6, 7]. Bifurcation diagrams show the dependence of the motion type on a relevant control parameter such as speed of rotation, rotor–stator clearance, etc.

Rotor–stator impact can be incorporated into computational models in several ways. The simplest approach is based on application of Newton's laws, as described in references [8–10], using a coefficient of restitution. Possible ways to determine practical values for the coefficient of restitution are described in reference [11]. Alternatively, contact behaviour can be modelled fairly simply by using a spring element to represent the contact stiffness, as described in references [5, 12]. However, friction and rotation of the shaft cross-section about axes perpendicular to the shaft centreline in the contact region are not taken into account in references [5, 12]. A more complete description of the contact problem can be obtained by using a finite element approach; see reference [13]. However, such a detailed model is not always the most suitable approach if the main aim is to obtain efficient computational predictions of overall system dynamics.

The aim of this paper is to contribute to the development of efficient methods for analyzing the dynamics of a rotor system in which contact occurs between rotor discs and the stationary parts of the system. Particular attention is paid to cases when both the discs of the rotor and the stator can be regarded as rigid bodies, and when the mass of the stationary part is considerably greater than mass of the rotor. Two modelling approaches have been developed and implemented in computer simulations. These are based on the application of Newton's laws and direct calculation of the impact forces. In the first approach, rotor–stator contact is modelled by using a coefficient of restitution. In the second approach, local flexibility and damping of the colliding bodies are considered. In general, these parameters depend on the deformation and rate of deformation of material in the neighbourhood of the contact area. Both methods take into account local flexibility between the discs and the shaft which allow not only linear displacement of the discs perpendicular to the shaft centreline but also their rotation about axes perpendicular to the shaft central line. The latter, novel feature allows the position of the point of contact between disc and casing to move axially according to disc rotation, which influences the moments exerted about the disc centre by the contact forces.

To solve the equations of motion of rotor systems numerically, the Runge–Kutta method is usually applied. Experience shows that a very short integration step is usually required to obtain satisfactory results, particularly when dealing with contact events. From the point of view of numerical stability the Newmark method is often advocated, but its basic algorithm, given for instance in reference [14], must be modified to make it possible to determine

explicitly the magnitudes and directions of radial and tangential components of impact forces during a contact event.

The next section of this paper deals with the formulation of the equations of motion and linearization of the resulting model. Two ways of incorporating impacts between the discs and the stationary part are then described. Finally, simulation results for the two models are presented and discussed.

2. EQUATIONS OF MOTION

In developing the lumped-parameter rotordynamic model, the system is assumed to have properties as outlined in the following. The shaft is represented as a flexible bar-like body, discretized into finite elements. The rotor rotates at constant angular speed, is rigid in torsion, and the friction forces that act on the discs during contact with the stator do not influence the speed of rotation. The shaft carries a number of discs that are attached to the shaft via connecting springs. These allow translation of the disc perpendicular to the shaft and rotation of the disc about diametral axes, perpendicular to the shaft, but are torsionally rigid. The discs are thin, rigid and circular, and run in cylindrical casings that are concentric with the undeflected shaft axis. Inertia and gyroscopic effects are taken into account in the shaft and disc models. Material damping is assumed to be viscous, and external damping linear. The bearings are modelled as hydrodynamic ones, the distribution of the oil pressure in the gap between the rotor journals and bearing housings being described by Reynolds equation. Finally, the rotor can be loaded by external force or kinematic inputs, which can be constant, or have harmonic or general time histories.

The lateral vibration of such rotor systems is described by equations of motion of the form

$$\mathbf{M}\ddot{\mathbf{x}} + (\mathbf{B} + \eta_V \mathbf{K}_{SH} + \Omega\mathbf{G})\dot{\mathbf{x}} + (\mathbf{K} + \Omega\mathbf{K}_C)\mathbf{x} = \mathbf{f} + \mathbf{f}_B(\mathbf{x}, \dot{\mathbf{x}}) \tag{1}$$

together with appropriate initial conditions, and boundary condition relationships of the form

$$\mathbf{x}_{BC} = \mathbf{x}_{BC}(t). \tag{2}$$

A complete listing of the notation is given in Appendix D.

The hydrodynamic fluid-film bearing forces are included in the computational model as a non-linear coupling-force vector, $\mathbf{f}_B$. The force magnitudes depend on the bearing geometry, the dynamic viscosity of the lubricant and on the relative displacements and velocities of the rotor journal and bearing housing centres.

Radial and tangential components of the bearing force acting on a rotor journal of length L and mean radius R are given by the integrals

$$F_{br} = -\int_0^{2\pi}\int_0^L p(\theta, x)R\cos\theta \, \mathrm{d}x\,\mathrm{d}\theta, \qquad F_{br} = -\int_0^{2\pi}\int_0^L p(\theta, x)R\sin\theta \, \mathrm{d}x\,\mathrm{d}\theta, \tag{3, 4}$$

where x is the co-ordinate in direction of the bearing axis and the meaning of angle θ is evident from Figure 1.

The distribution of the oil pressure p along the circumference and length of the bearing gap results from solving Reynold's equation and depends on boundary conditions. Solution in a closed form can be obtained only in special cases, see references [3, 4].

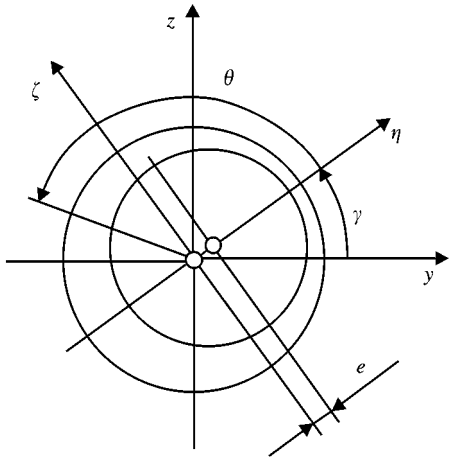

Figure 1. Geometry of the hydrodynamic bearing.

To obtain elements of vector $\mathbf{f}_B$ the radial and tangential components of the bearing forces equations (3) and (4) must be resolved into the fixed frame of reference by using the transformation

$$F_{by} = F_{br}\cos\gamma - F_{bt}\sin\gamma, \qquad F_{bz} = F_{br}\sin\gamma + F_{bt}\cos\gamma, \tag{5, 6}$$

where angle γ (see Figure 1) must satisfy the trigonometric equations

$$\cos\gamma = \frac{y_J - y_B}{\sqrt{(y_J - y_B)^2 + (z_J - z_B)^2}}, \qquad \sin\gamma = \frac{z_J - z_B}{\sqrt{(y_J - y_B)^2 + (z_J - z_B)^2}}. \tag{7, 8}$$

The resulting vector of bearing forces $\mathbf{f}_B$ can be expanded into a Taylor series in the neighbourhood of the static position, as

$$\mathbf{f}_B(\mathbf{x}, \dot{\mathbf{x}}) = \mathbf{f}_{BST} + \mathbf{D}_B\dot{\mathbf{x}} + \mathbf{D}_K(\mathbf{x} - \mathbf{x}_{ST}) + \cdots, \tag{9}$$

where

$$\mathbf{f}_{BST} = \mathbf{f}_B(\mathbf{x}_{ST}, \mathbf{0}), \qquad \mathbf{D}_B = \left[\frac{\partial \mathbf{f}_B(\mathbf{x}, \dot{\mathbf{x}})}{\partial \dot{\mathbf{x}}}\right]_{\mathbf{x} = \mathbf{x}_{ST}, \dot{\mathbf{x}} = 0}, \qquad \mathbf{D}_K = \left[\frac{\partial \mathbf{f}_B(\mathbf{x}, \dot{\mathbf{x}})}{\partial \mathbf{x}}\right]_{\mathbf{x} = \mathbf{x}_{ST}, \dot{\mathbf{x}} = 0} \tag{10–12}$$

If displacements and velocities of the rotor journal centre from the equilibrium position are small relative to the bearing clearance, terms of second and higher order in the Taylor series (9) can be neglected. Under this condition, after substituting equation (9) into equation (1), the following some manipulation, the linearized equation of motion becomes

$$\mathbf{M}\cdot\ddot{\mathbf{x}} + (\mathbf{B} + \eta_V\cdot\mathbf{K}_{SH} + \Omega\cdot\mathbf{G} - \mathbf{D}_B)\cdot\dot{\mathbf{x}} + (\mathbf{K} + \Omega\cdot\mathbf{K}_C - \mathbf{D}_K)\cdot\mathbf{x} = \mathbf{f}_{ST} + \mathbf{f}_A(t) + \mathbf{f}_{BST} - \mathbf{D}_K\cdot\mathbf{x}_{ST}. \tag{13}$$

From the physical point of view the negative of matrices $\mathbf{D}_B$ and $\mathbf{D}_K$ express the linearized stiffness and damping properties of the fluid-film bearings.

A necessary step in the linearization process is to determine the static position of the rotor system by solving the following set of non-linear algebraic equations for the elements of vector $\mathbf{x}_{ST}$:

$$(\mathbf{K} + \Omega \cdot \mathbf{K}_C) \cdot \mathbf{x}_{ST} = \mathbf{f}_{ST} + \mathbf{f}_B(\mathbf{x}_{ST}, \mathbf{0}). \tag{14}$$

After introducing the substitution

$$\mathbf{f}_{STC} = \mathbf{f}_{ST} + \mathbf{f}_{BST} - \mathbf{D}_K \mathbf{x}_{ST} \tag{15}$$

the linearized equation of motion (13) is transformed to

$$\mathbf{M}\ddot{\mathbf{x}} + (\mathbf{B} + \eta_V \cdot \mathbf{K}_{SH} + \Omega \cdot \mathbf{G} - \mathbf{D}_B)\dot{\mathbf{x}} + (\mathbf{K} + \Omega \cdot \mathbf{K}_C - \mathbf{D}_K)\mathbf{x} = \mathbf{f}_{STC} + \mathbf{f}(t), \tag{16}$$

where the vector $\mathbf{f}_{STC}$ follows from equations (14) and (15) as

$$\mathbf{f}_{STC} = (\mathbf{K} + \Omega \mathbf{K}_C - \mathbf{D}_K)\mathbf{x}_{ST}. \tag{17}$$

As previously mentioned, impacts between the discs and the stationary part will be modelled in two ways as described in the following sections.

2.1. APPROACH BASED ON APPLICATION OF NEWTON'S IMPACT THEORY

To apply Newton's impact theory, the following additional properties are assigned to the model rotor system. The discs and the rotor casing are taken to be absolutely rigid bodies and the effective mass of the casing is considerably greater than the mass of particular discs. Dissipation of mechanical energy due to deformation of the colliding bodies is taken into account by means of the coefficient of restitution, and Coulomb friction opposes slipping motion in the contact area. It is assumed that the rotor speed is such that the circumferential velocity of the disc is the dominant component of the relative velocity between the colliding bodies at the point of contact. Consequently, the Coulomb friction force acts on the disc in a circumferential direction, which is determined entirely by the direction of rotation of the rotor. For investigation of individual impact events, it is assumed that the centre of mass of the disc is coincident with its geometric centre.

The rigid discs have four degrees of freedom (d.o.f.s), i.e., the linear displacements in the y and z directions and rotations about axes parallel to y and z. The discs are connected to the shaft through isotropic spring elements having lateral and bending stiffness in two mutually perpendicular directions. The springs have a physical meaning because they represent a mounting stiffness (effectively a contact stiffness) between the disc and shaft. From the modelling viewpoint the springs are particularly convenient, because they decouple the disc from the shaft at the moment of the impact, thus allowing simple application of Newton's impact theory.

It will be assumed that, during the contact period, the impact forces are considerably greater than all other forces acting on the colliding bodies, including the forces and moments transmitted by the spring elements connecting the discs and the shaft.

The geometry of the system during impact is evident from Figure 2, which also identifies the radial and tangential components of contact force, F_{rr}, F_{rt}, acting on the disc. The centre, C, of the disc is shifted radially and its central plane is turned resulting in axial displacement of impact point R. To describe the impact, the rotated frame of reference, $O_{\xi\eta\zeta}$, is introduced. Axis $O\eta$ passes through centres of the disc and the casing and

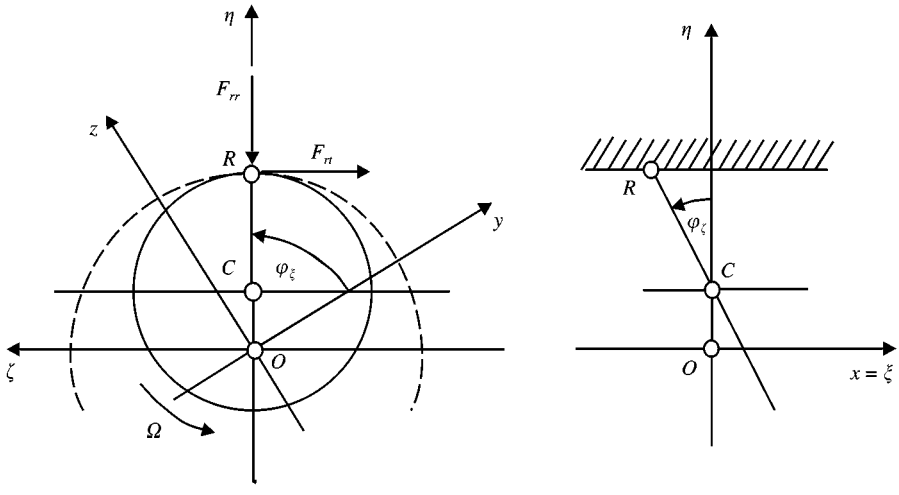

Figure 2. Disc geometry and contact force components.

through the impact point R. Axis $O\xi$ is coincident with axis Ox and $O\zeta$ is perpendicular to $O\xi$ an $O\eta$.

To analyze the problem, the y and z components of the velocity of the disc centre, and the angular velocity of the disc, must be transformed into the rotated frame of reference as follows:

$$\dot{\eta}_C = \dot{y}_C \cos\varphi_\xi + \dot{z}_C \sin\varphi_\xi, \qquad \dot{\zeta}_C = -\dot{y}_C \sin\varphi_\xi + \dot{z}_C \cos\varphi_\xi, \tag{18, 19}$$

$$\dot{\varphi}_\eta = \dot{\varphi}_y \cos\varphi_\xi + \dot{\varphi}_z \sin\varphi_\xi, \qquad \dot{\varphi}_\zeta = -\dot{\varphi}_y \sin\varphi_\xi + \dot{\varphi}_z \cos\varphi_\xi. \tag{20, 21}$$

Here the angle φ_ξ, which defines the instantaneous swash angle of the disc, is a solution of the two equations

$$\cos\varphi_\xi = \frac{y_C}{\sqrt{y_C^2 + z_C^2}}, \qquad \sin\varphi_\xi = \frac{z_C}{\sqrt{y_C^2 + z_C^2}}. \tag{22, 23}$$

According to Newton's theory, the period of impact has two phases that are separated by an instant of time when the normal component of the relative velocity of the colliding bodies at the point of impact is zero.

Upon taking into account the assumption that mass of the disc is considerably smaller than the mass of the stationary part, components of the disc velocity after the impact can be determined by solving the following set of equations, which will be discussed later:

$$m_D(\dot{\eta}_{C0} - \dot{\eta}_{C1}) = -\int_0^{T_0} F_{rr}(t)\,\mathrm{d}t, \qquad m_D(\dot{\eta}_{C2} - \dot{\eta}_{C0}) = -\int_{T_0}^{T_R} F_{rr}(t)\,\mathrm{d}t, \tag{24, 25}$$

$$J_D(\dot{\varphi}_{\zeta 0} - \dot{\varphi}_{\zeta 1}) = R_D\varphi_\zeta \int_0^{T_0} F_{rr}(t)\,\mathrm{d}t, \qquad J_D(\dot{\varphi}_{\zeta 2} - \dot{\varphi}_{\zeta 0}) = R_D\varphi_\zeta \int_{T_0}^{T_R} F_{rr}(t)\,\mathrm{d}t, \tag{26, 27}$$

$$\dot{\eta}_{C0} - R_D \varphi_\zeta \dot{\varphi}_{\zeta 0} = 0, \qquad \varepsilon_R = \int_{T_0}^{T_R} F_{rr}(t)\,\mathrm{d}t \Big/ \int_0^{T_0} F_{rr}(t)\,\mathrm{d}t \tag{28, 29}$$

$$F_{rt} = \mu F_{rr} s, \quad m_D(\dot{\zeta}_{C2} - \dot{\zeta}_{C1}) = -\int_0^{T_R} F_{rt}(t)\,\mathrm{d}t, \quad J_D(\dot{\varphi}_{\eta 2} - \dot{\varphi}_{\eta 1}) = -R_D \varphi_\zeta \int_0^{T_R} F_{rt}(t)\,\mathrm{d}t. \tag{30–32}$$

Equations (24), (25) and (31) govern the change of the disc's linear momentum during impact in the radial and tangential directions and equations (26), (27) and (32) govern the change in its moment of momentum. Equation (28) expresses the relationship between the translational and angular velocities of the disc at the point in time separating the first and second phases of the impact. Equation (29) defines the coefficient of restitution and equation (30) expresses Coulomb's law for friction.

Parameter s depends on the direction and orientation of the friction force. Upon noting that the tangential component of the velocity of the disc at the impact point, immediately before impact, is given by

$$\dot{\zeta}_{R1} = \dot{\zeta}_{C1} + R_D \Omega, \tag{33}$$

then s takes values as follows:

$$s = 1 \quad \text{if } \dot{\zeta}_{R1} > 0, \quad s = 0, \quad \text{if } \dot{\zeta}_{R1} = 0, \quad s = -1 \quad \text{if } \dot{\zeta}_{R1} < 0. \tag{34}$$

Because the angular velocity, Ω, of the rotor is usually high, the second term on the right-hand side of equation (33) is considerably greater than the first so that

$$\dot{\zeta}_{C1} \ll R_D \Omega, \tag{35}$$

in which case equation (33) can be rewritten into the approximate form

$$\dot{\zeta}_{R1} \doteq R_D \Omega. \tag{36}$$

The magnitudes of the velocity components of the disc immediately after the impact, obtained in the rotated frame of reference, must be transformed to the fixed frame as

$$\dot{y}_C = \dot{\eta}_C \cos\varphi_\xi - \dot{\zeta}_C \sin\varphi_\xi, \qquad \dot{z}_C = \dot{\eta}_C \sin\varphi_\xi + \dot{\zeta}_C \cos\varphi_\xi, \tag{37, 38}$$

$$\dot{\varphi}_y = \dot{\varphi}_\eta \cos\varphi_\xi - \dot{\varphi}_\zeta \sin\varphi_\xi, \qquad \dot{\varphi}_z = \dot{\varphi}_\eta \sin\varphi_\xi + \dot{\varphi}_\zeta \cos\varphi_\xi. \tag{39, 40}$$

Impact of the disc with the casing occurs if the following geometric and kinematic conditions are satisfied:

$$\eta_C - R_D(1 - \cos\varphi_\zeta) = \delta, \qquad \dot{\eta}_C - R_D \varphi_\zeta \dot{\varphi}_\zeta > 0. \tag{41, 42}$$

The velocities of the discs after the impact are calculated by using equations (37)–(40), and the new acceleration magnitudes are determined from

$$\ddot{\mathbf{x}}_2 = \mathbf{M}^{-1}[\mathbf{f}_{STC} + \mathbf{f}(t) - (\mathbf{B} + \eta_V \mathbf{K}_{SH} + \Omega \mathbf{G} - \mathbf{D}_B)\dot{\mathbf{x}}_2 - (\mathbf{K} + \Omega \mathbf{K}_C - \mathbf{D}_K)\mathbf{x}]. \tag{43}$$

To take account of the boundary conditions the equation of motion is transformed to the form

$$\mathbf{A}_2 \ddot{\mathbf{y}} + \mathbf{A}_1 \dot{\mathbf{y}} + \mathbf{A}_0 \mathbf{y} = \mathbf{b}, \tag{44}$$

where matrices $\mathbf{A}_0$, $\mathbf{A}_1$, $\mathbf{A}_2$ and vectors $\mathbf{y}$, $\dot{\mathbf{y}}$, $\ddot{\mathbf{y}}$, $\mathbf{b}$ are obtained from $\mathbf{A}_0^*$, $\mathbf{A}_1^*$, $\mathbf{A}_2^*$, $\mathbf{x}$, $\dot{\mathbf{x}}$, $\ddot{\mathbf{x}}$, $\mathbf{b}^*$ (defined below) by removing the rows and columns that correspond to those degrees of freedom for which the boundary conditions are prescribed:

$$\mathbf{A}_2^* = \mathbf{M}, \qquad \mathbf{A}_1^* = \mathbf{B} + \eta_V \mathbf{K}_{SH} + \Omega \mathbf{G} - \mathbf{D}_B, \qquad \mathbf{A}_0^* = \mathbf{K} + \Omega \mathbf{K}_C - \mathbf{D}_K, \quad (45\text{–}47)$$

$$\mathbf{b}^* = \mathbf{f}_{STC} + \mathbf{f}(t) - \mathbf{M}\ddot{\mathbf{x}}_{BC} - (\mathbf{B} + \eta_V \mathbf{K}_{SH} + \Omega \mathbf{G} - \mathbf{D}_B)\dot{\mathbf{x}}_{BC} - (\mathbf{K} + \Omega \mathbf{K}_C - \mathbf{D}_K)\mathbf{x}_{BC}. \quad (48)$$

To solve the modified equation of motion, equation (44), the Newmark method was applied in a modified form (see Appendix A). After each integration time step, a check was performed to determine whether or not contact had occurred, using the conditions

$$\eta_{C,t+\Delta t} - R_D(1 - \cos \varphi_{\zeta,t+\Delta t}) \geqslant \delta, \qquad \dot{\eta}_{C,t+\Delta t} - R_D \varphi_{\varsigma,t+\Delta t} \dot{\varphi}_{\varsigma,t+\Delta t} > 0. \quad (49, 50)$$

The physical nature of the problem dictates that the time step, Δt, must be very short, so that there is no need for a more complex, iterative procedure to determine the instant of impact with sufficient accuracy. When an impact happens, the post-impact magnitudes of velocities and accelerations of the rotor system are determined before the next integration step is performed.

2.2. APPROACH BASED ON DETERMINATION OF IMPACT FORCES

The second modelling approach is based on direct determination of contact forces acting between the colliding bodies during impact. This is achieved by modelling the local radial deformation behaviour at the point of contact by using an assumed contact stiffness in parallel with a viscous damping element. As before, Coulomb friction is assumed to act at the point of contact, the friction force acting on the disc in the circumferential direction.

The impact force has radial and tangential components (see Figure 2), both of which depend on local contact stiffness and damping and on the geometric and kinematic parameters of the colliding bodies, as follows:

$$F_{rr} = F_{conr} = -k_{con}[\eta_C - R_D(1 - \cos \varphi_\zeta) - \delta] - b_{con}(\dot{\eta}_C - R_D \varphi_\varsigma \dot{\varphi}_\varsigma), \quad (51)$$

$$F_{rt} = F_{cont} = -k_{con}[\eta_C - R_D(1 - \cos \varphi_\zeta) - \delta]\mu s - b_{con}(\dot{\eta}_C - R_D \varphi_\varsigma \dot{\varphi}_\varsigma)\mu s. \quad (52)$$

Here s is given by equation (34) and k_{con} and b_{con} are defined below.

If, during the period of impact, the disc undergoes angular displacement about a diametral axis, the contact force produces a bending moment acting on the disc. It has two components given by

$$M_{conr} = F_{cont} R_D \varphi_\zeta, \qquad M_{cont} = -F_{conr} R_D \varphi_\zeta, \quad (53, 54)$$

which act about axes parallel to F_{rt} and F_{rr} respectively.

The power dissipated by the friction force is given by

$$P_F = F_{rt}(\dot{\zeta}_C + R_D \Omega), \quad (55)$$

which can be approximated as follows if the speed of rotation of the rotor, Ω, is high:

$$\mathbf{P}_F \doteq F_{rt} R_D \Omega. \quad (56)$$

In general, the contact stiffness and damping are complex functions of strain and strain rate in the deformation zone and thus depend on the displacement and velocity of the disc centre in the radial direction so that

$$k_{con} = k_{con}(\eta_C, \dot{\eta}_C), \qquad b_{con} = b_{con}(\eta_C, \dot{\eta}_C). \tag{57, 58}$$

In the simplest case k_{con} and b_{con} can be considered as constant, and the damping coefficient b_{con} is often expressed as a multiple of the contact stiffness

$$b_{con} = \beta_{con} k_{con}. \tag{59}$$

Before incorporation of components of the impact forces and moments into the equation of motion they must be transformed from the rotated to the fixed frame of reference, by using the same transformation as that used in equations (37)–(40), so that

$$F_{cony} = F_{conr}\cos\varphi_\xi - F_{cont}\sin\varphi_\xi, \qquad F_{conz} = F_{conr}\sin\varphi_\xi + F_{cont}\cos\varphi_\xi, \tag{60, 61}$$

$$M_{cony} = M_{conr}\cos\varphi_\xi - M_{cont}\sin\varphi_\xi, \qquad M_{conz} = M_{conr}\sin\varphi_\xi + M_{cont}\cos\varphi_\xi, \tag{62, 63}$$

where angle φ_ξ satisfies equations (22) and (23) at the appropriate point of time.

Following the above analysis, the equation of motion can be written as

$$\mathbf{M}\cdot\ddot{\mathbf{x}} + (\mathbf{B} + \eta_V\mathbf{K}_{SH} + \Omega\mathbf{G} - \mathbf{D}_B)\dot{\mathbf{x}} + (\mathbf{K} + \Omega\mathbf{K}_C - \mathbf{D}_K)\mathbf{x} = \mathbf{f}_{STC} + \mathbf{f}(t) + \mathbf{f}_{CON}(\mathbf{x}, \dot{\mathbf{x}}). \tag{64}$$

To take the boundary conditions into account, equation (64) can be written as

$$\mathbf{A}_2\ddot{\mathbf{y}} + \mathbf{A}_1\dot{\mathbf{y}} + \mathbf{A}_0\mathbf{y} = \mathbf{b}(\mathbf{y}, \dot{\mathbf{y}}), \tag{65}$$

where matrices $\mathbf{A}_0$, $\mathbf{A}_1$, $\mathbf{A}_2$ and vectors $\mathbf{y}$, $\dot{\mathbf{y}}$, $\ddot{\mathbf{y}}$ are as defined for equation (44) and $\mathbf{b}$ results from vector $\mathbf{b}^*$, given below, by omitting those elements for which boundary conditions are prescribed:

$$\mathbf{b}^* = \mathbf{f}_{STC} + \mathbf{f}(t) - \mathbf{M}\ddot{\mathbf{x}}_{BC} - (\mathbf{B} + \eta_V\mathbf{K}_{SH} + \Omega\mathbf{G} - \mathbf{D}_B)\dot{\mathbf{x}}_{BC} - (\mathbf{K} + \Omega\mathbf{K}_C - \mathbf{D}_K)\mathbf{x}_{BC} + \mathbf{f}_{CON}. \tag{66}$$

Equation (65) is non-linear because vector $\mathbf{b}$ is a function of displacements and velocities. For its solution a modified Newmark algorithm was used, as outlined in Appendix B. The principal problem with its application is how to express the vector of impact forces $\mathbf{f}_{CON}$ at point of time $t + \Delta t$, because the kinematic parameters are not yet calculated at this time. As before, the physical nature of the problem requires the use a short integration time step Δt. Therefore, the simplest possibilities are either to use the kinematic parameters obtained at previous integration step (i.e., at time t), in which case

$$\mathbf{f}_{CON}(t + \Delta t) \doteq \mathbf{f}_{CON}[\mathbf{x}(t), \dot{\mathbf{x}}(t)], \tag{67}$$

or to assume that the rotor motion during the short time interval is uniformly accelerated so that

$$\mathbf{f}_{CON}(t + \Delta t) \doteq \mathbf{f}_{CON}[\mathbf{x}(t) + \Delta t\dot{\mathbf{x}}(t) + \tfrac{1}{2}\Delta t^2\ddot{\mathbf{x}}(t),\ \dot{\mathbf{x}}(t) + \Delta t\ddot{\mathbf{x}}]. \tag{68}$$

Before performing each integration step, the conditions of impact

$$\eta_C - R_D(1 - \cos\varphi_\zeta) \geqslant \delta, \qquad F_{conr} \leqslant 0, \tag{69, 70}$$

must be inspected for all discs and new values of contact forces calculated as required. The force condition (70) is introduced to avoid physically unrealizable tensile contact forces acting between the discs and the stationary part. These can be predicted if, as when a viscoelastic contact model is used, the contact forces are assumed to depend on the rate of deformation of material in the neighbourhood of the impact point.

3. APPLICATION EXAMPLES

The above modelling schemes will now be illustrated by application to two examples. These are based on the system shown in Figure 3, for which relevant geometrical and physical parameter values are given in Appendix C. The system consists of a shaft, which

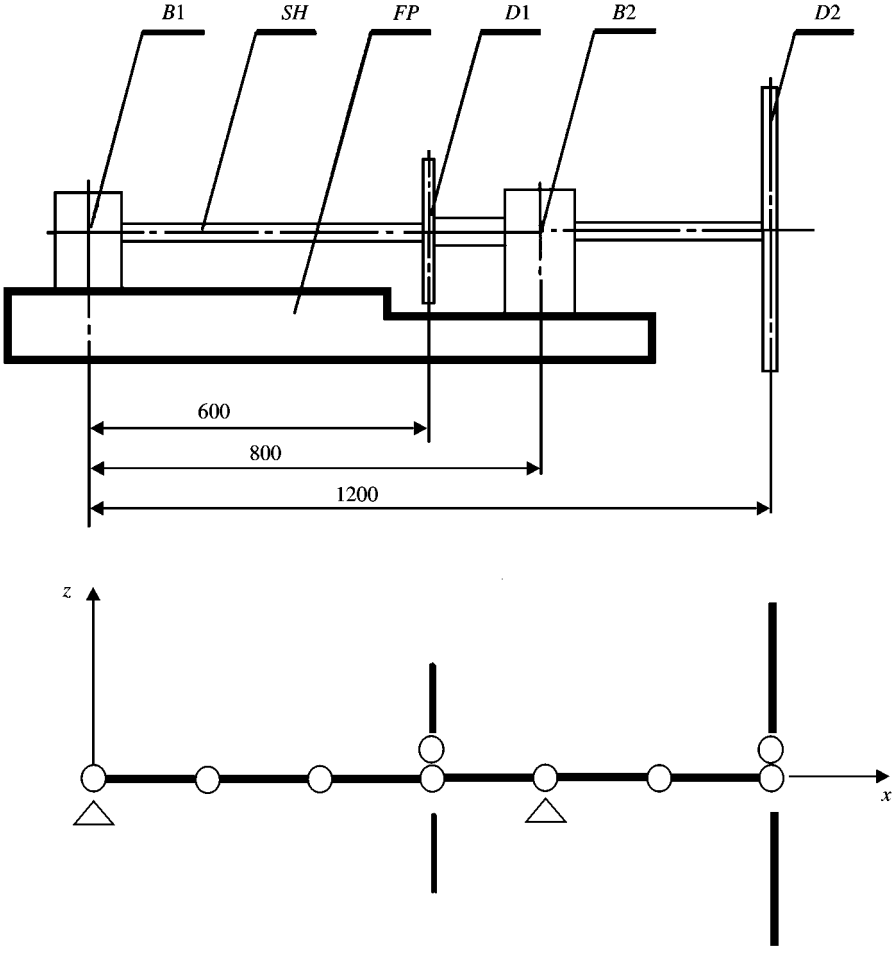

Figure 3. Schematic of the example rotor system. Legend: B1, B2—bearings, D1, D2—discs, SH—shaft, FP—foundation plate.

TABLE 1

Eigenvalues (rad/s) at different angular speeds of rotation

	$\Omega = 250$ rad/s	$\Omega = 500$ rad/s	$\Omega = 750$ rad/s	$\Omega = 1000$ rad/s
n		λ_n (rad/s)		
1.	$-34{\cdot}2 \pm 126{\cdot}7i$	$-34{\cdot}3 \pm 251{\cdot}2i$	$-32{\cdot}7 \pm 376{\cdot}2i$	$-28{\cdot}5 \pm 502{\cdot}3i$
2.	$-87{\cdot}4 \pm 137{\cdot}0i$	$-97{\cdot}7 \pm 261{\cdot}8i$	$-93{\cdot}4 \pm 389{\cdot}4i$	$-75{\cdot}2 \pm 522{\cdot}9i$
3.	$-9{\cdot}8 \pm 625{\cdot}5i$	$-9{\cdot}3 \pm 615{\cdot}0i$	$-8{\cdot}4 \pm 605{\cdot}2i$	$-7{\cdot}7 \pm 595{\cdot}3i$
4.	$-13{\cdot}9 \pm 642{\cdot}9i$	$-19{\cdot}2 \pm 651{\cdot}6i$	$-27{\cdot}0 \pm 658{\cdot}2i$	$-46{\cdot}2 \pm 658{\cdot}6i$
5.	$-40{\cdot}1 \pm 2061{\cdot}4i$	$-51{\cdot}0 \pm 2044{\cdot}1i$	$-49{\cdot}3 \pm 2029{\cdot}9i$	$-46{\cdot}1 \pm 2017{\cdot}1i$
6.	$-74{\cdot}6 \pm 2067{\cdot}6i$	$-76{\cdot}4 \pm 2083{\cdot}7i$	$-84{\cdot}7 \pm 2096{\cdot}9i$	$-93{\cdot}9 \pm 2108{\cdot}5i$

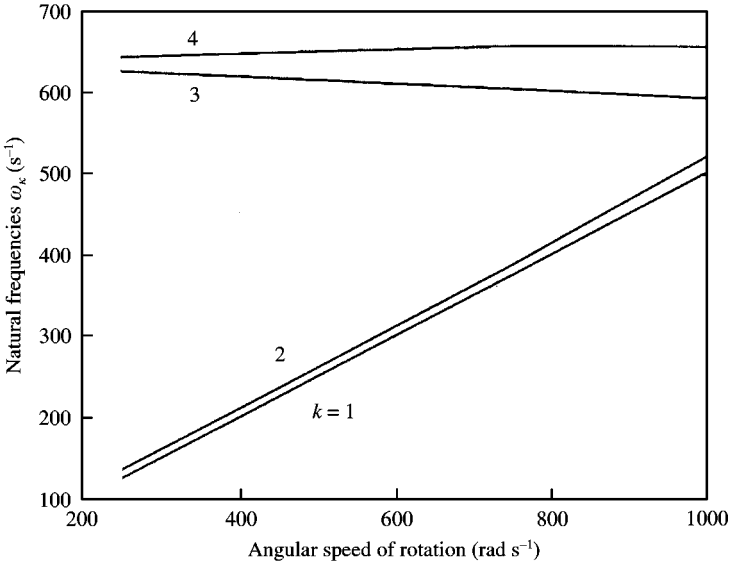

Figure 4. Dependence on rotor speed of imaginary part of eigenvalues of example rotor system.

supports two discs, and is coupled to a rigid foundation plate through two hydrodynamic bearings. The shaft rotates at constant speed and the overhung disc runs in a cylindrical housing.

For the purpose of the calculation the model rotor was discretized by using six finite elements. The discs were considered to be thin and absolutely rigid and both bearings as short and fully cavitated. Dead load of the rotor was taken into account.

For reference, the complex eigenvalues of the system at a range of shaft speeds are given in Table 1, from which it can be seen that the system is stable. Figure 4 shows the dependence of the first two pairs of system natural frequencies on shaft speed and illustrates the expected splitting of these pairs due to gyroscopic coupling. The effect of increasing bearing stiffness on the lowest natural frequencies as the shaft speed increases is clearly visible.

3.1. EXAMPLE 1

In this example, the shaft was loaded by a concentrated radial force, of constant magnitude and direction, acting at the location of disc D1. In addition, a suddenly applied

imbalance force was assumed to act on disc D2, equivalent to a centre-of-mass eccentricity of 1·0 mm, represented by two, mutually perpendicular harmonic forces acting on the shaft in the plane of disc D2. The aim was to investigate the influence of the width of the clearance between disc D2 and its housing on the response of the rotor system. The first mentioned

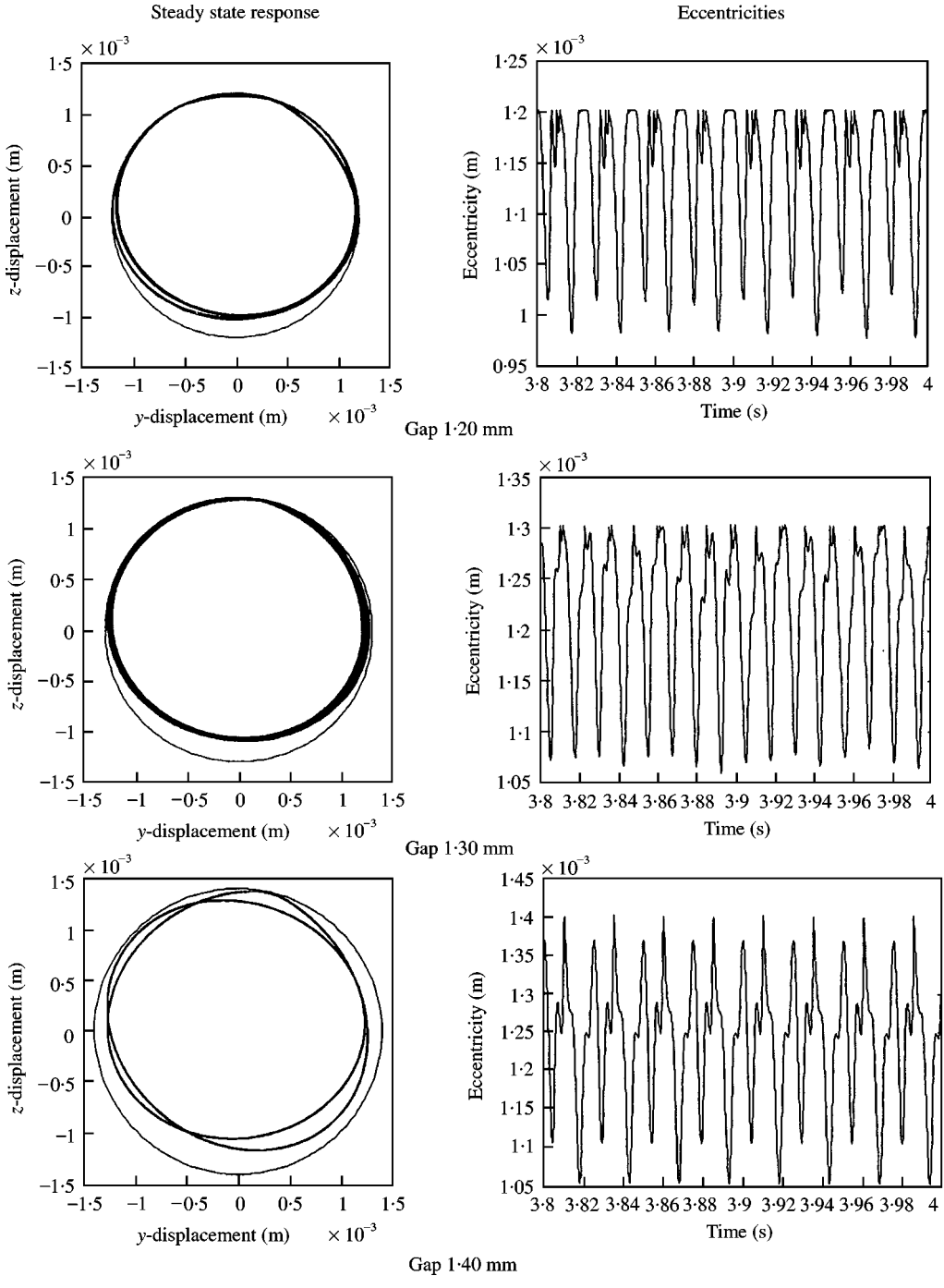

Figure 5. Orbits of centre of disc D2 and time histories of eccentricity for various initial clearance gaps.

modelling approach was used and the coefficients of restitution and Coulomb friction for contact between disc D2 and its housing were taken to be 0·8 and 0·2 respectively. The shaft speed was 500 rad/s.

Some representative results of the numerical simulations, all relating to the period when the vibration can be considered as steady state, are given in Figures 5–9. Figure 5 shows the

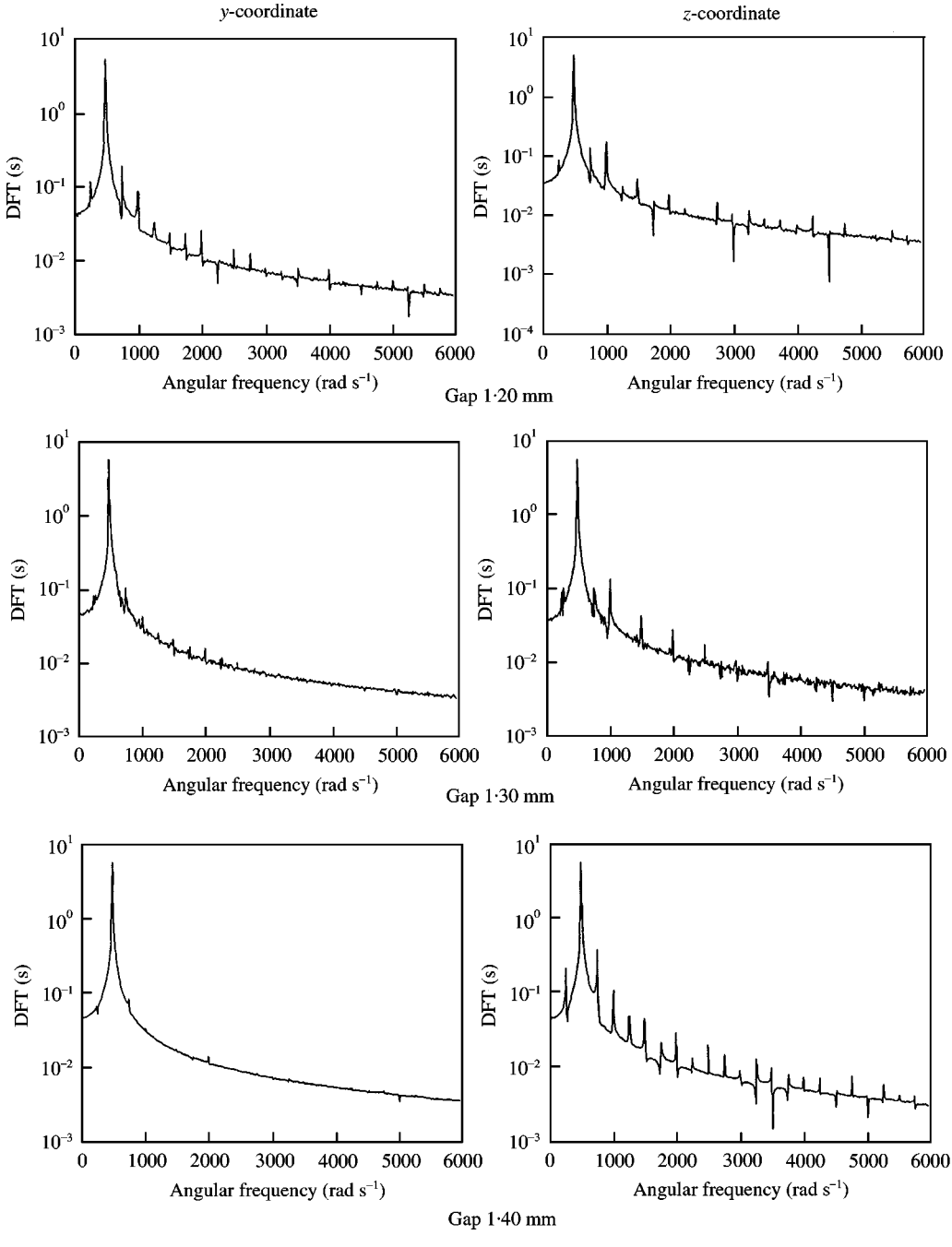

Figure 6. DFT of displacement of centre of disc D2.

orbit of the centre of disc D2 and corresponding time series of its eccentricity for three values of the rotor-casing clearance. With 1·2 mm initial clearance there is almost continuous sliding contact between the disc and certain sections of the casing. With 1·4 mm initial clearance, the steady state vibration of the rotor is periodic. During the simulation period only one impact occurs.

Figure 6 shows the Fourier transforms of time series of y and z displacement components of the centre of disc D2. The principal contributions to the steady state response are formed

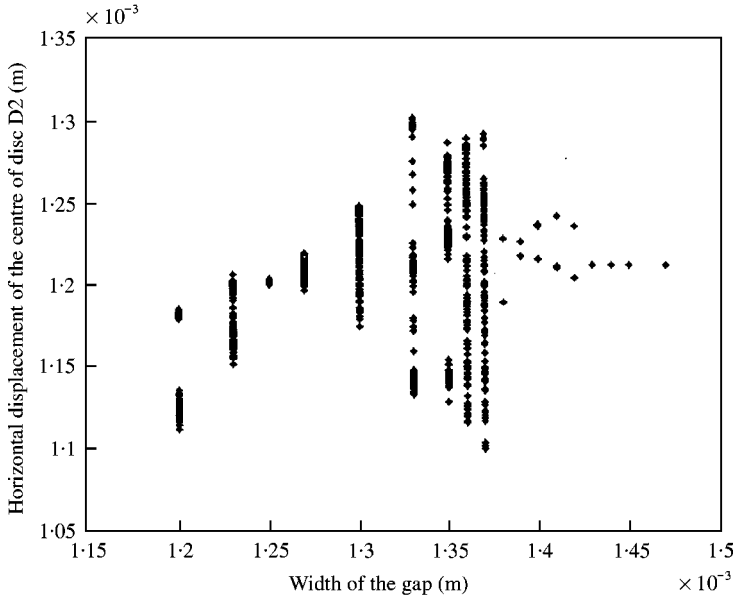

Figure 7. Bifurcation diagram based on horizontal displacement of centre of disc D2.

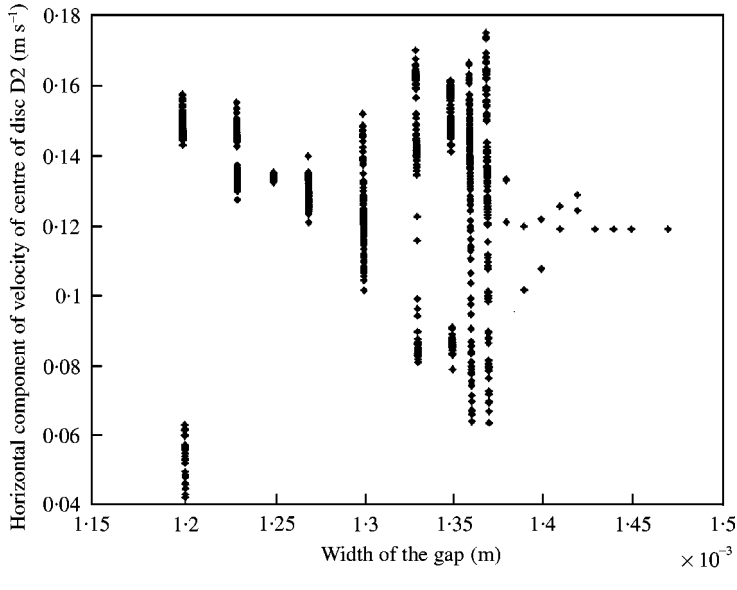

Figure 8. Bifurcation diagram based on horizontal velocity of centre of disc D2.

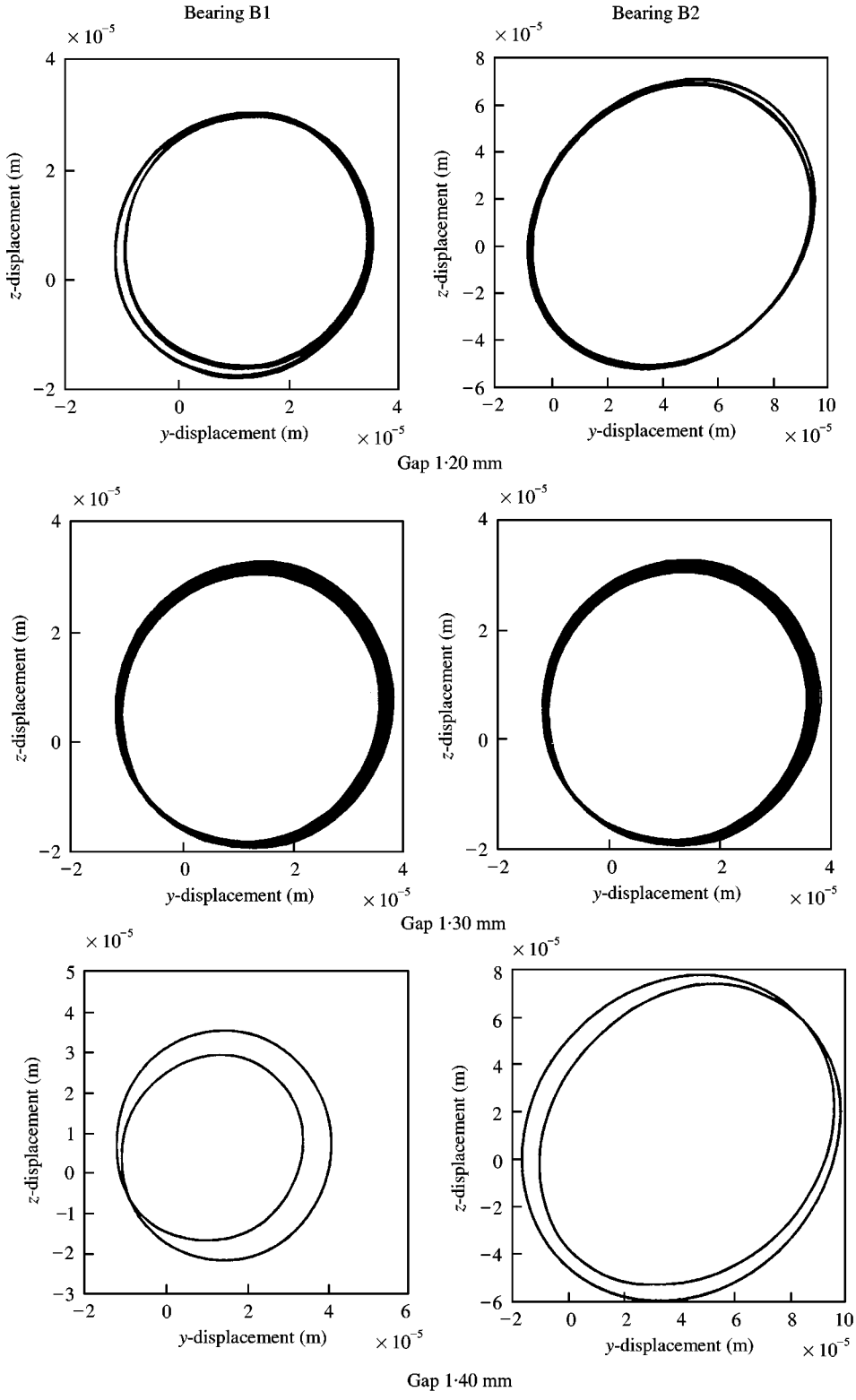

Figure 9. Orbits of bearing centres under mass imbalance excitation.

by partial motions with frequencies corresponding to integer multiples of one-half of the frequency of excitation. In all cases investigated the dominant frequency in the spectra is equal to the excitation frequency due to mass imbalance corresponding to the shaft speed

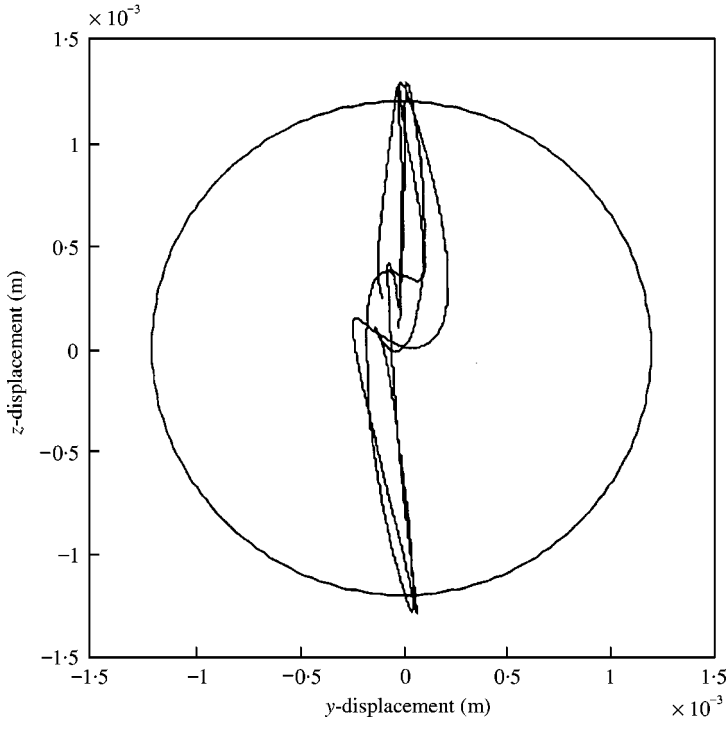

Figure 10. Trajectory of centre of disk D2 under vertical displacement excitation of base plate.

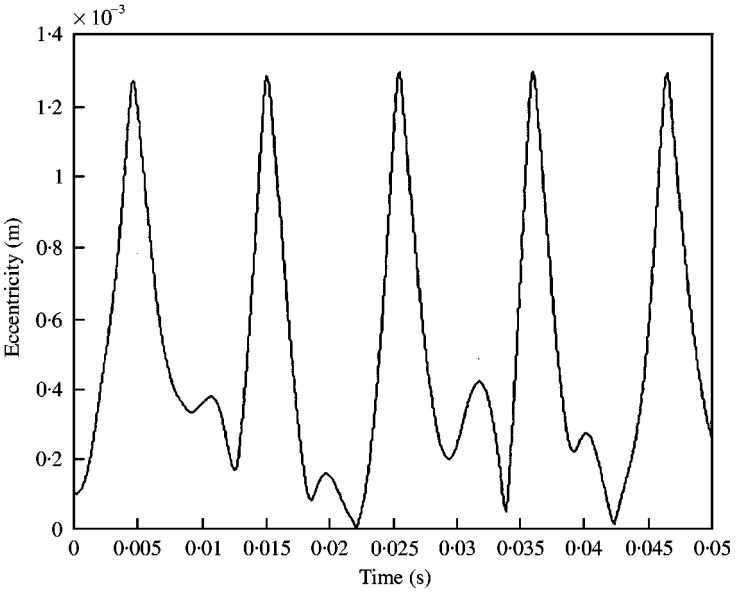

Figure 11. Time history of eccentricity of centre of disk D2 under vertical displacement excitation of base plate.

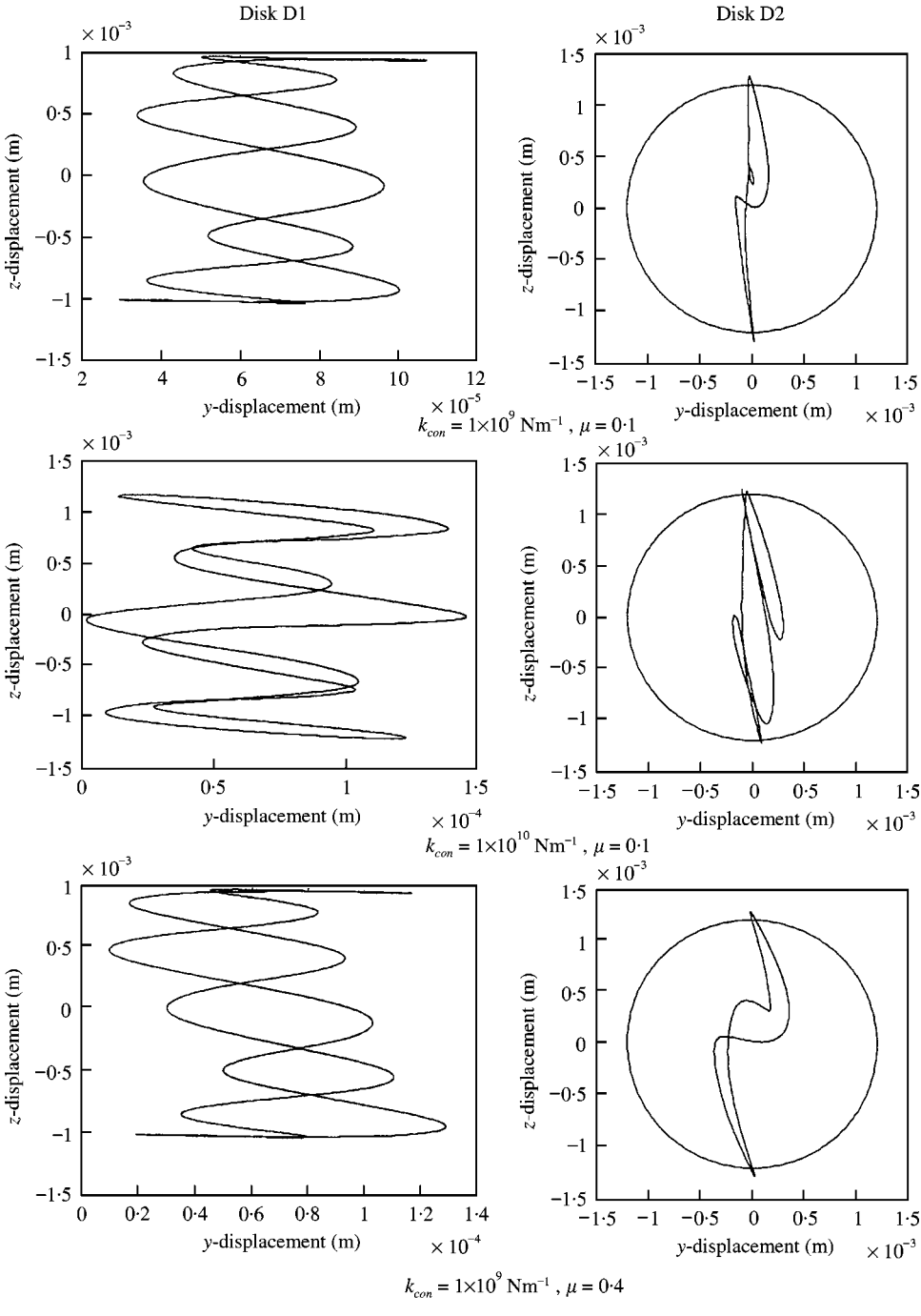

Figure 12. Effect of contact stiffness and coefficient of friction on steady state orbits of centres of discs D1 and D2 under vertical displacement excitation of base plate.

500 rad/s. When the initial clearance is 1·3 mm, the frequency spectrum has a broadband character that is characteristic of chaotic motion.

Figure 7 is a bifurcation diagram representing the dependence of the y displacement of the centre of disc D2, determined at the end of each rotor revolution, on the initial

rotor–stator clearance. For clearances between 1·37 and 1·42 mm, the steady state vibration is $2T$-periodic where T is the period of excitation. When the clearance is greater, the motion becomes $1T$ periodic. However, if the clearance is lower, then the vibration becomes quasi-periodic or even chaotic (i.e., hardly predictable). The behaviour of the z-component of displacement shows the same trends. The same pattern of behaviour is observed in

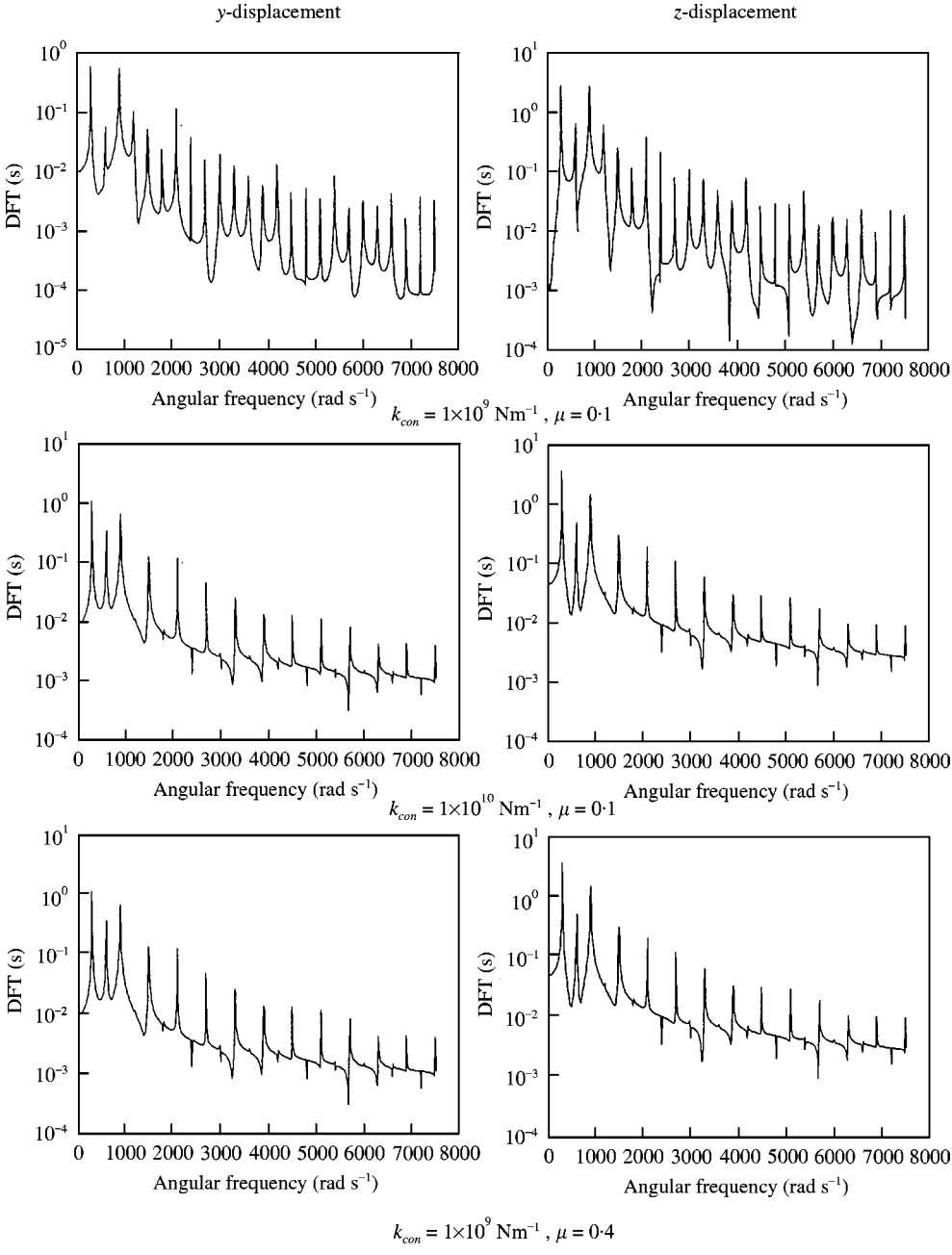

Figure 13. Effect of contact stiffness and coefficient of friction on DFT of displacement of centre of disc D2.

Figure 8 based on the y-component of velocity of the centre of disc D2 at the end of each revolution of the rotor.

The forms of the trajectories of the rotor journal centres in bearings B1 and B2 are evident from Figure 9. It is clear that their displacements from the static position can be considered small with respect to the bearing gap (0·2 mm), justifying the use of the approach based on linearization of the stiffness and damping properties of the fluid-film bearings.

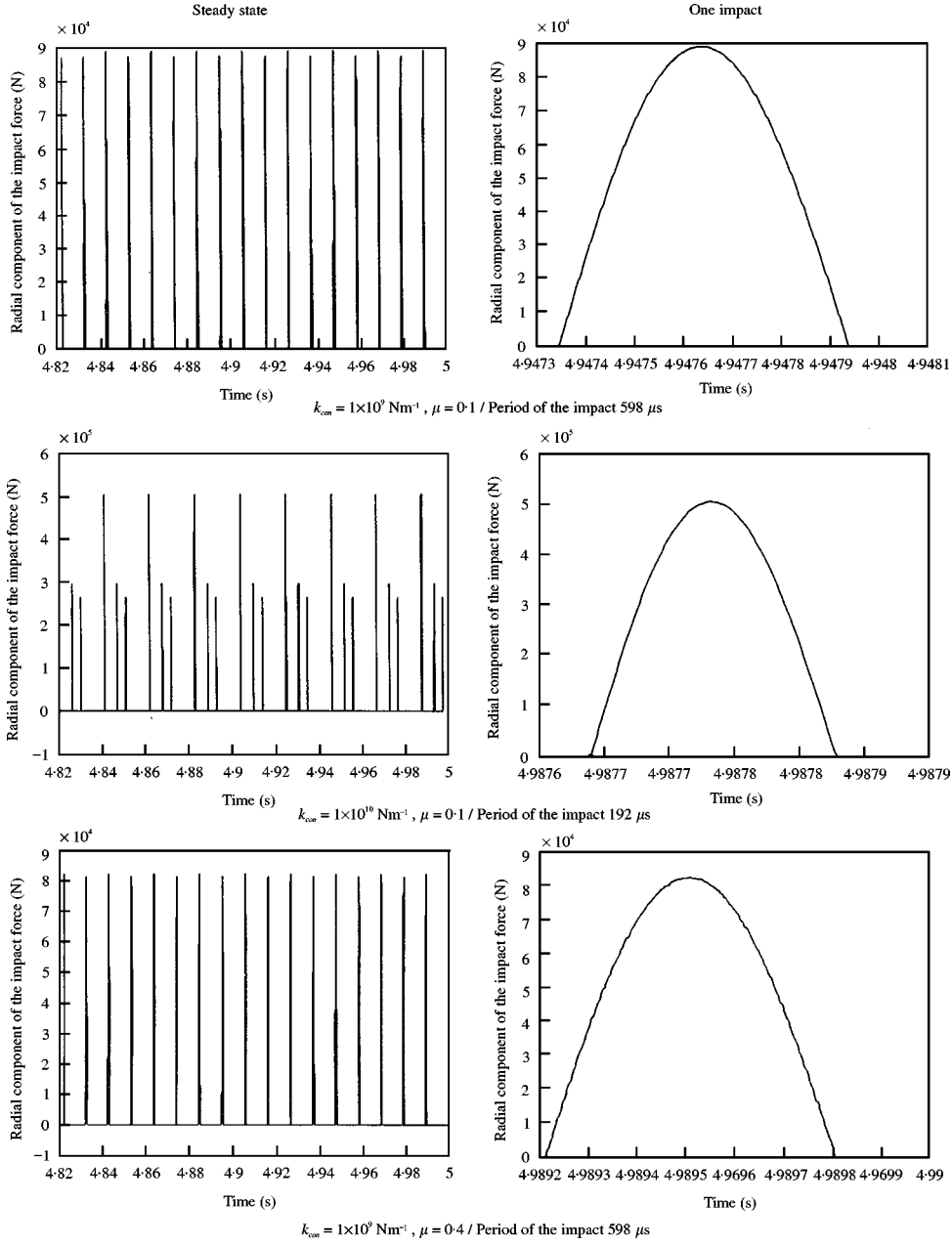

Figure 14. Effect of contact stiffness and coefficient of friction on time history of radial impact force D2 under vertical displacement excitation of base plate.

3.2. EXAMPLE 2

The second modelling approach is demonstrated here for the case in which the system is excited kinematically. The foundation plate was subjected to a vertical harmonic displacement with 1·0 mm amplitude and angular frequency 300 rad/s. In this case, the influence of the contact stiffness and coefficient of friction at the rotor-casing contact were

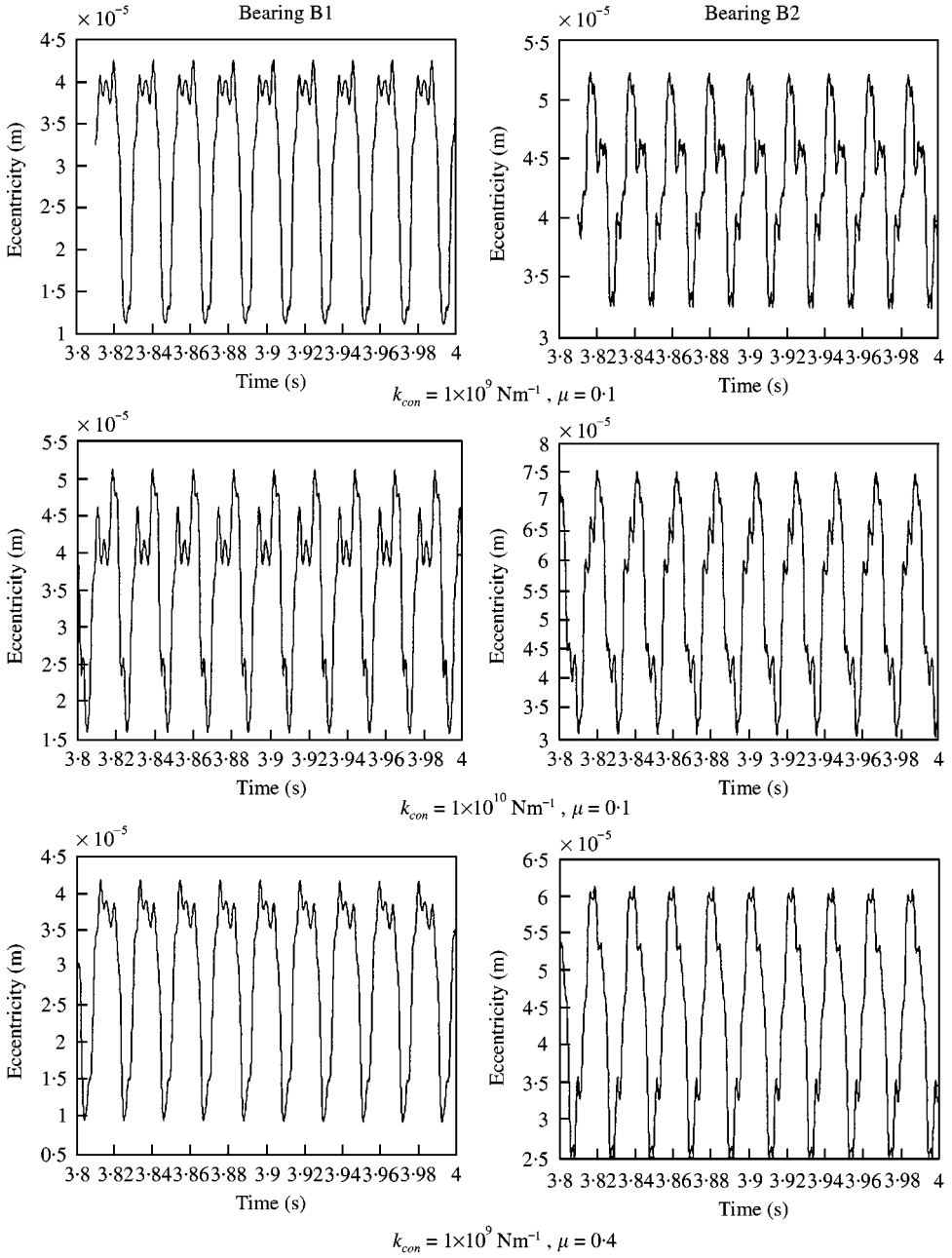

Figure 15. Effect of contact stiffness and coefficient of friction on time history of bearing centre eccentricities under vertical displacement excitation of base plate.

studied. Reference values of these parameters, assumed constant, were chosen as follows: contact stiffness $k_{con} = 1 \times 10^9$ N/m, based on Hertzian contact theory (Note that this is two orders of magnitude smaller than the radial stiffness of the disc-to-shaft connection spring, see Appendix C); coefficient of friction $\mu = 0{\cdot}1$. The coefficient of proportionality between viscous damping and contact stiffness (equation (59)) was assumed to be 1×10^{-7} s and the shaft speed was again taken as 500 rad/s. The principal results are summarized in Figures 10–15.

Figures 10 and 11 show the initial trajectory and corresponding time history of the eccentricity of the centre of disc D2 when the excitation is applied. The displacement of the disc centre slightly exceeds the initial rotor–stator clearance. This is due to two factors; (i) local deformation of the colliding bodies (contact stiffness) and (ii) because of turning of the disc central plane around axes perpendicular to the shaft central line, as permitted by flexibility of the shaft and of the disc-to-shaft mounting.

The forms of orbits of the centres of discs D1 and D2 are shown in Figure 12 for a range of values of contact stiffness and Coulomb friction coefficient. The results correspond to the period when the transient component of the vibration has already died out. In all the illustrated cases the steady state vibration is periodic. It is evident that the studied parameters influence the form of the trajectory of the investigated nodes. For example, increasing the contact stiffness from 10^9 to 10^{10} N/m changes the number of impacts during one excitation period from two to three. (Note the different scales in the vertical and horizontal directions.)

Fourier transforms of the steady state time histories of the y and z components of the response of the centre of disc D2 are shown in Figure 13, for a range of contact parameters. In all cases, the dominant frequencies correspond to integer multiples of the excitation frequency (300 rad/s). Figure 14 shows time histories of radial component of the impact force during the corresponding period of steady state vibration. Increasing the contact stiffness by a factor of 10 reduces the period of duration of the impact by a factor of $\sim \sqrt{10}$, as expected, and increases the maximum value of the impact force. However, it may be noted that the combination of these two factors does not produce a large change in the impulse of the impact force. Increasing the coefficient of Coulomb friction from 0·1 to 0·4 has little influence on the magnitude of the radial component of the impact force and duration of the impacts. The time histories of the power dissipation during contact, due to friction forces, have shapes that are identical to the radial force time histories shown in Figure 14, the instantaneous power being obtained by multiplying the radial contact force by the coefficient of Coulomb friction and the sliding velocity.

Time histories of the relative eccentricities of the rotor journal centres in bearings B1 and B2 are shown in Figure 15. The maximum changes in eccentricity in the bearings resulting from base-plate excitation are no greater than about 15% of the bearing clearance in the cases considered, again indicating the acceptability of the modelling approach based on linearization of the stiffness and damping properties of the bearings.

4. CONCLUSIONS

Investigation of the behaviour of rotor systems in which impacts occur between the rotor and its housing is an interesting problem for which several modelling approaches can be used.

Procedures based on the application of Newton's theory and on the direct calculation of the contact forces have been developed and tested. Both approaches make it possible to investigate lateral vibration of the rotor system from the point of view of the limit state of

deformation that is determined by the width of the gap between the rotor and the stationary part, to determine frequency of the impacts during the transition or steady state phase of the motion and consider character of the steady state vibration (periodic, quasi-periodic, chaotic). For this purpose knowledge of forms of trajectories, Poincaré maps, bifurcation diagrams or Lyapunov exponents are needed. The second procedure provides some additional information e.g., on the magnitude and time history of the impact force or on time of duration of the impacts. The applicability of the methods has been illustrated by examples involving imbalance and baseplate excitations.

ACKNOWLEDGMENT

This research work has been supported by the Ministry of Education of the Czech Republic (research project CEZ:J17/98:2724019) and by the Grant Agency of the Czech Republic (grant no. 101/99/1327). Their help is gratefully acknowledged.

REFERENCES

1. H. D. NELSON and J. M. MCVAUGH 1976 *Transactions of the American Society of Mechanical Engineers, Journal of Engineering for Industry* **May**, 593–600. The dynamics of rotor-bearing systems using finite elements.
2. E. S. ZORZI and H. D. NELSON 1977 *Transactions of the American Society of Mechanical Engineers, Journal of Engineering for Power* **January**, 71–76. Finite element simulation of rotor-bearing systems using finite elements.
3. E. KRÄMER 1993 *Dynamics of Rotors and Foundations*, Berlin: Springer-Verlag.
4. J. M. VANCE 1988 *Rotordynamics of Turbomachinary*, New York: John Wiley & Sons, Inc.
5. M. F. A. AZEEZ and A. F. VAKAKIS 1999 *International Journal of Non-linear Mechanics* **34**, 415–435. Numerical and experimental analysis of a continuous overhung rotor undergoing vibro-impacts.
6. F. C. MOON 1987 *Chaotic Vibrations. An Introduction for Applied Scientists and Engineers*, New York: John Wiley & Sons, Inc.
7. F. PETERKA 1992 *Journal of Sound and Vibration* **154**, 95–115. Transitions to chaotic motion in mechanical systems with impacts.
8. J. ZAPOMĚL and E. MALENOVSKÝ 1999 *Zeszyty naukowe Katedry mechaniky stosowanej* **1999**, 83–86. Numerical investigation of rotors supported by nonlinear bearings using Newton's theory.
9. J. ZAPOMĚL and E. MALENOVSKÝ 1999 *Proceedings of European Conference on Computational Mechanics* '99, *August* 31–*September* 3, CD. Methods for numerical investigation of vibration of rotors with impacts on the stationary part. Munich.
10. M. K. K. GHAURI, C. H. J. FOX and E. J. WILLIAMS 1996 *Proceedings of the VIth International Conference on Vibrations in Rotating Machinery*, 383–394. Transient response and contact due to sudden imbalance in a flexible rotor-casing system with support asymmetry., I. Mech. E, Oxford.
11. L. PŮST 1998 *Engineering Mechanics* **5**, 303–318. Equivalent coefficient of restitution.
12. C. H. J. FOX, E. J. WILLIAMS and Y. L. CHEN 1998 *Proceedings of the International Conference on Multi-Body Dynamics*, 191–200. A linear model for impact between a rigid body and an elastic ring. I. Mech. E, London.
13. Z.-H. ZHONG 1993 *Finite Element Procedures for Contact-Impact Problems.* Oxford: Oxford University Press.
14. K. SUBBARAJ and M. A. DOKAINISH 1989 *Computers and Structures* **32**, 1387–1401. A survey of direct time-integration methods in computational structural dynamics—II. Implicit methods.

APPENDIX A: ALGORITHM 1

Given: β, γ—coefficients of the Newmark method,

Δt—time step.

1. Determination of constants of the Newmark method:

$$a_0 = \frac{1}{\beta \Delta t^2}, \qquad a_4 = \frac{\gamma}{\beta} - 1,$$

$$a_1 = \frac{\gamma}{\beta \Delta t}, \qquad a_5 = \frac{\Delta t}{2}\left(\frac{\gamma}{\beta} - 2\right),$$

$$a_2 = \frac{1}{\beta \Delta t}, \qquad a_6 = \Delta t(1 - \gamma),$$

$$a_3 = \frac{1}{2\beta} - 1, \qquad a_7 = \gamma \Delta t.$$

2. Determination of modified coefficient matrices:

$$\mathbf{A}_0, \mathbf{A}_1, \mathbf{A}_2.$$

3. Calculation of the initial accelerations:

$$\ddot{\mathbf{y}}_0 = \mathbf{A}_2^{-1}[\mathbf{b}_0 - \mathbf{A}_1 \dot{\mathbf{y}}_0 - \mathbf{A}_0 \mathbf{y}_0].$$

4. Determination of the matrix of effective stiffness:

$$\mathbf{A}_{ef} = \mathbf{A}_0 + a_0 \mathbf{A}_2 + a_1 \mathbf{A}_1.$$

5. Set-up of the vector of effective load:

$$\mathbf{b}_{ef,t+\Delta f} = \mathbf{b}_{t+\Delta t} + \mathbf{A}_2(a_0 \mathbf{y}_t + a_2 \dot{\mathbf{y}}_t + a_3 \ddot{\mathbf{y}}_t) + \mathbf{A}_1(a_1 \mathbf{y}_t + a_4 \dot{\mathbf{y}}_t + a_5 \ddot{\mathbf{y}}_t).$$

6. Calculation of displacements at point of time $t + \Delta t$:

$$\mathbf{A}_{ef} \mathbf{y}_{t+\Delta t} = \mathbf{b}_{ef,t+\Delta t}.$$

7. Calculation of accelerations and velocities at point of time $t + \Delta t$:

$$\ddot{\mathbf{y}}_{t+\Delta t} = a_0(\mathbf{y}_{t+\Delta t} - \mathbf{y}_t) - a_2 \dot{\mathbf{y}}_t - a_3 \ddot{\mathbf{y}}_t, \qquad \dot{\mathbf{y}}_{t+\Delta t} = \dot{\mathbf{y}}_t + a_6 \ddot{\mathbf{y}}_t + a_7 \ddot{\mathbf{y}}_{t+\Delta t}.$$

8. Conditions of impact for all discs:

$$\eta_{C,t+\Delta t} - R_D(1 - \cos \varphi_{\zeta,t+\Delta t}) \geqslant \delta, \qquad \dot{\eta}_{C,t+\Delta t} - R_D \varphi_{\varsigma,t+\Delta t} \dot{\varphi}_{\varsigma,t+\Delta t} > 0.$$

If the conditions are not satisfied, go to 11.

9. Calculation of new velocities $\dot{\mathbf{y}}_{t+\Delta t}$ of the colliding discs after the impacts.
10. Calculation of new accelerations of the system after the impact:

$$\ddot{\mathbf{y}}_{t+\Delta t} = \mathbf{A}_2^{-1} \cdot [\mathbf{b}_0 - \mathbf{A}_1 \dot{\mathbf{y}}_{t+\Delta t} - \mathbf{A}_0 \mathbf{y}_{t+\Delta t}].$$

11. $t + \Delta t \to t, \qquad \mathbf{y}_{t+\Delta t} \to \mathbf{y}_t, \qquad \dot{\mathbf{y}}_{t+\Delta t} \to \dot{\mathbf{y}}_t, \qquad \ddot{\mathbf{y}}_{t+\Delta t} \to \ddot{\mathbf{y}}_t;$

Return to 5.

APPENDIX B: ALGORITHM 2

Given: β, γ—coefficients of the Newmark method,

Δt—time step.

1. Determination of constants of the Newmark method:

$$a_0 = \frac{1}{\beta \Delta t^2}, \qquad a_4 = \frac{\gamma}{\beta} - 1,$$

$$a_1 = \frac{\gamma}{\beta \Delta t}, \qquad a_5 = \frac{\Delta t}{2}\left(\frac{\gamma}{\beta} - 2\right),$$

$$a_2 = \frac{1}{\beta \Delta t}, \qquad a_6 = \Delta t(1 - \gamma),$$

$$a_3 = \frac{1}{2\beta} - 1, \qquad a_7 = \gamma \Delta t.$$

2. Determination of modified coefficient matrices:

$$\mathbf{A}_0, \mathbf{A}_1, \mathbf{A}_2.$$

3. Calculation of the initial accelerations:

$$\ddot{\mathbf{y}}_0 = \mathbf{A}_2^{-1}[\mathbf{b}_0 - \mathbf{A}_1 \dot{\mathbf{y}}_0 - \mathbf{A}_0 \mathbf{y}_0].$$

4. Determination of the matrix of effective stiffness:

$$\mathbf{A}_{ef} = \mathbf{A}_0 + a_0 \mathbf{A}_2 + a_1 \mathbf{A}_1.$$

5. Calculation of the vector of impact forces:

$$\mathbf{b}_{con, t+\Delta t} = \mathbf{b}_{con}(\mathbf{y}_t, \dot{\mathbf{y}}_t).$$

6. Set up of the vector of effective load:

$$\mathbf{b}_{ef, t+\Delta t} = \mathbf{b}_{t+\Delta t} + \mathbf{A}_2(a_0 \mathbf{y}_t + a_2 \dot{\mathbf{y}}_t + a_3 \ddot{\mathbf{y}}_t) + \mathbf{A}_1(a_1 \mathbf{y}_t + a_4 \dot{\mathbf{y}}_t + a_5 \ddot{\mathbf{y}}_t) + \mathbf{b}_{con, t+\Delta t}.$$

7. Calculation of displacements at point of time $t + \Delta t$:

$$\mathbf{A}_{ef} \mathbf{y}_{t+\Delta t} = \mathbf{b}_{ef, t+\Delta t}.$$

8. Calculation of accelerations and velocities at point of time $t + \Delta t$:

$$\ddot{\mathbf{y}}_{t+\Delta t} = a_0(\mathbf{y}_{t+\Delta t} - \mathbf{y}_t) - a_2 \dot{\mathbf{y}}_t - a_3 \ddot{\mathbf{y}}_t, \qquad \dot{\mathbf{y}}_{t+\Delta t} = \dot{\mathbf{y}}_t + a_6 \ddot{\mathbf{y}}_t + a_7 \ddot{\mathbf{y}}_{t+\Delta t}.$$

9. $t + \Delta t \to t$, $\mathbf{y}_{t+\Delta t} \to \mathbf{y}_t$, $\dot{\mathbf{y}}_{t+\Delta t} \to \dot{\mathbf{y}}_t$, $\ddot{\mathbf{y}}_{t+\Delta t} \to \ddot{\mathbf{y}}_t$;
Return to 5.

APPENDIX C: GEOMETRICAL AND PHYSICAL PARAMETERS OF THE MODEL SYSTEMS

Shaft

Element 1	length	200 mm	diameter	100 mm
Element 2	length	200 mm	diameter	100 mm
Element 3	length	200 mm	diameter	130 mm
Element 4	length	200 mm	diameter	150 mm
Element 5	length	200 mm	diameter	80 mm
Element 6	length	200 mm	diameter	80 mm

Young's modulus $2{\cdot}1 \times 10^{11}$ N/m^2
Density 7800 kg/m^3
Coefficient of viscous damping $2{\cdot}0 \times 10^{-7}$ s

Discs	*Disc* 1	*Disc*2
Mass	24 kg	32kg
Radius	0·15 m	0·25 m
Diametral moment of inertia	0·09 kg m^2	0·12 kg m^2
Polar moment of inertia	0·18 kg m^2	0·25 kg m^2

Disc-to-shaft spring elements
Longitudinal stiffness 1×10^{11} N/m
Bending stiffness 1×10^{11} N m/rad

Rayleigh coefficients for external damping

$\alpha = 5, \qquad \beta = 0.$

Bearings

Radius	60 mm
Length	150 mm
Bearing clearance	0.2 mm
Oil viscosity	0·04 Pa s

*Static load at disc D*2
y (horizontal) component 12 000 N
z (vertical) component 20 000 N

APPENDIX D: NOMENCLATURE

Matrices

$\mathbf{M}, \mathbf{K}$	mass, stiffness matrices of the rotor system
$\mathbf{B}$	damping matrix (external damping, material damping of the stator)
$\mathbf{D}_B$	partial derivatives with respect to elements of vector $\dot{\mathbf{x}}$
$\mathbf{D}_K$	partial derivatives with respect to elements of vector $\mathbf{x}$
$\mathbf{G}, \mathbf{K}_C$	gyroscopic, circulation matrices of the rotor
$\mathbf{K}_{SH}$	stiffness matrix of the shaft

Vectors

$\mathbf{f}$	generalized forces
$\mathbf{f}_{ST}$	static loading forces
$\mathbf{f}_A$	time-varying forces (including applied and constant forces)
$\mathbf{f}_B$	bearing forces
$\mathbf{f}_{BST}$	bearing forces at equilibrium position of the rotor
$\mathbf{f}_{CON}$	contact (impact) forces
$\mathbf{x}, \dot{\mathbf{x}}, \ddot{\mathbf{x}}$	generalized displacements, velocities, accelerations
$\mathbf{x}_{ST}$	generalized displacements at equilibrium position
$\mathbf{x}_{BC}, \dot{\mathbf{x}}_{BC}, \ddot{\mathbf{x}}_{BC}$	boundary conditions (displacements, velocities, accelerations)
$\dot{\mathbf{x}}_2, \ddot{\mathbf{x}}_2$	generalized velocities, accelerations after impact
$\mathbf{0}$	zero vector

Scalars, vector components

F_{br}, F_{bt}	radial, tangential components of bearing force acting on rotor journal
F_{by}, F_{bz}	y, z components of bearing force acting on rotor journal
F_{rr}, F_{rt}	radial, tangential components of impact force acting on rotor
F_{conr}, F_{cont}	radial, tangential components of impact force acting on rotor

F_{cony}, F_{conz}	y, z components of the impact force acting on rotor
J_D	moment of inertia of the disc (with respect to its diameter)
k_{con}, b_{con}	contact stiffness, coefficient of damping in the contact area
M_{conr}, M_{cont}	radial, tangential components of moment of impact force acting on rotor
M_{cony}, M_{conz}	y, z components of moment of impact force acting on rotor
m_D	mass of the disc
P_F	power of the friction (tangential component of the impact) force
R_D	radius of the disc
T_R, T_0	time of duration of the impact, of the first phase of the impact
t, Δt	time, time step (increment)
y_j, z_j	y, z displacements of the rotor journal centre
y_B, z_B	y, z displacements of the bearing housing centre
y_C, z_C	y, z, η, ζ displacements of the disc centre C

β_{con}	coefficient of proportionality
δ	width of the gap between the disc and the stationary part
ε_R	coefficient of restitution
η_V	coefficient of viscous damping
η_C, ζ_C	η, ζ displacements of the disc centre C
φ_y,φ_z, φ_η, φ_ζ	rotation of the disc around axes y, z, parallel to η, ζ
ζ_{RV}	tangential component of velocity of the disc at impact point R
μ	coefficient of friction
Ω	rotor angular velocity

overdots denote differentiation with respect to time.